

Self-supervised Learning for Clustering of Wireless Spectrum Activity

Ljupcho Milosheski^a, Gregor Cerar^a, Blaž Bertalaníč^a, Carolina Fortuna^a, Mihael Mohorčič^a

^a*Jozef Stefan Institute, Department of Communication Technologies, Jamova Cesta 39, 1000, Ljubljana, Slovenia*

Abstract

In recent years, much work has been done on processing of wireless spectrum data involving machine learning techniques in domain-related problems for cognitive radio networks, such as anomaly detection, modulation classification, technology classification and device fingerprinting. Most of the solutions are based on labeled data, created in a controlled manner and processed with supervised learning approaches. However, spectrum data measured in real-world environment is highly nondeterministic, making its labeling a laborious and expensive process, requiring domain expertise, thus being one of the main drawbacks of using supervised learning approaches in this domain. In this paper, we investigate the use of self-supervised learning (SSL) for exploring spectrum activities in a real-world unlabeled data. In particular, we compare the performance of two SSL models, one based on a reference DeepCluster architecture and one adapted for spectrum activity identification and clustering, and a baseline model based on K-means clustering algorithm. We show that SSL models achieve superior performance regarding the quality of extracted features and clustering performance. With SSL models we achieve reduction of the feature vectors size by two orders of magnitude, while improving the performance by a factor of 2 to 2.5 across the evaluation metrics, supported by visual assessment. Additionally we show that adaptation of the reference SSL architecture to the domain data provides reduction of model complexity by one order of magnitude, while preserving or even improving the clustering performance.

Keywords: spectrum, analysis, clustering, self-supervised, machine learning
2010 MSC: 90B20

1. Introduction

The number and type of wireless devices connected to the Internet is rapidly increasing with the current affordable personal mobile and Internet of Things (IoT) devices, requiring wireless networks to handle large number of connections and high traffic loads. As a reference, the requirement for the number of connected devices in the fifth-generation (5G) networks is one million devices per square kilometer. The existence of such a number of devices requires complex wireless resource management. Over time, several new approaches to wireless resource sharing, including dynamic spectrum access [1], licensed shared access [2] have been proposed. However, additional technological components, such as spectrum usage databases [3] and radio environment maps [4], had to be developed to enable such sophisticated and dynamic spectrum usage approaches. To be able to correctly inform on spectrum usage, additional knowledge of other devices operating within the range of a wireless device is critical for future smart usage of the spectrum. In this respect, some of the recent efforts were focused on detecting the modulation used [5], technology used [6], anomalous activities [7], etc.

As also discussed in [8] and [9], significant effort is still being invested in the field to develop accurate and scalable deep learning algorithms able to accurately and automatically manage spectrum resource usage. With respect to the learning approach, these techniques can be divided into (1) *supervised* that require labels to be present for the training data, and (2) *unsupervised* that do not assume any such labels. Applications

in wireless spectrum management need to be aware of operating details (i.e., type of technology, transmission parameters, etc.). Development of a deep-learning based model to support such application typically requires labelled data that is expensive to acquire as it requires complex wireless and computing equipment [10, 11] or intense labelling efforts by domain experts [12] that do not always lead to high quality labels due to nondeterministic nature of wireless operating environments. *Semi-supervised* and *active-learning* emerged as alternative techniques that have the advantage of using a relatively small amount of labeled samples for achieving performance that is comparable to the regular supervised approach.

Given the advent of large datasets which are expensive or practically impossible to label, *self-supervised learning* (SSL) [13], as another intermediate learning approach, is becoming an important alternative that is particularly suitable to reduce the data labelling cost and leverage the unlabelled data pool. SSL is a representation learning method where a supervised task is created out of the unlabelled data. Using an SSL approach, it is possible to create very similar groups (i.e. clusters) from a large, unlabelled dataset and then label each cluster. By labelling the learnt clusters, it is possible to then use the model as a classifier by assigning new, unseen examples to those clusters and therefore label them as one would do in a typical classification task.

Developing an easy to use, automated and technology agnostic way to explore spectrum activities and group similar activities, eventually enabling automatic rather than manual trans-

mission identification and cataloging as currently done for instance in the Signal Identification Guide¹, is still an open research topic which motivated this investigation.

In this paper, we investigate the suitability of SSL to support automatic spectrum exploration on an example of an unlicensed 868 MHz Short Range Device (SRD) band in an urban environment using 15 days of spectrum sweeps collected in a wireless testbed LOG-a-TEC². Leveraging this data, we propose a new SSL architecture adapted for spectrum activity identification and clustering, in which segments of spectrograms containing signal activity are used to train the deep learning (DL) self-supervised network and enable the discovery of the types of transmissions available over the respective period of time. It is based on machine vision and inspired by DeepCluster [14], which is also used in this study as a reference SSL model. We experimentally prove that such an architecture is suitable for spectrogram analysis by learning spectrum features and clustering spectrograms based on their content. The performance of SSL models is also compared to a baseline approach using Principal Component Analysis (PCA) for feature extraction and K-means as the clustering algorithm.

The main contributions of this work can be summarised as follows:

- Adaptation of an SSL architecture to discover wireless transmissions in real-world spectrogram data when no prior knowledge (i.e. labels) is available, while also achieving significant reduction of the complexity of the architecture with 12 times less trainable parameters compared to the selected baseline.
- Proposing dimensionality reduction of the output of the convolutional neural network (CNN) by PCA using a threshold on the amount of explained variance ratio (EVR), achieving features quality and clustering performance improvement by a factor of 2-2.5 across the selected evaluation metrics.
- Experimental evaluation of the adapted SSL architecture for two use cases, activity detection and fine grain transmissions classification.

The rest of the paper is structured as follows. Section 2 analyzes the related work, Section 3 introduces SSL and baseline system architectures, Section 4 elaborates on the experimental methodology and Section 5 presents the experimental results. Finally, Section 6 concludes the paper.

2. Related work

In recent years, as in many other research areas the use of deep learning models gained a lot of attention also in the development of algorithms for processing spectrum data. Selected works from the domain which are considered as most relevant

and closely related to this paper are listed in Table 1, which summarizes their main characteristics, and briefly elaborate in the following where they are grouped according to the adopted learning approach.

2.1. Supervised learning

In the existing works, *supervised* DL-based models are most widely represented and they achieve significant increase of performance when compared to more traditional ML approaches, as shown in [6], [17], [16].

In [6], the authors compare the performance and generalization ability of models that use manually extracted expert features with models that use raw spectrum data. They are solving the task of technology classification on a dataset containing transmissions of three different wireless technologies. They prove that using CNN on raw In-Phase and Quadrature (I/Q) data or spectrogram images outperforms all other models in terms of accuracy, generalization ability to unseen datasets from different operating environments, and robustness to different noise levels.

In [16], an application of CNN supervised learning for device identification, again using raw I/Q data, is proposed. The dataset contains transmissions from five devices. Device identification is based on the CNN's ability to learn various device-specific impairments in the raw signals. SVM and logistic regression are used as reference models for performance comparison and authors show that the proposed CNN model significantly outperforms the baseline algorithms for the posed task.

In many cases, state-of-the-art accuracy is achieved by adopting and modifying DL-based architectures that are already known and well established in other, closely related signal processing fields, such as image and sound processing [15], [7]. In [20], device classification task using real-world I/Q data of transmissions from a large population of nearly 10,000 devices is solved using a new neural network architecture based on dilated causal convolutional layers. The design is motivated by an existing audio signals processing architecture.

2.2. Semi-supervised and transfer learning

Although the supervised models have superior performance judging by their accuracy, the necessity for large labeled training datasets as one of the major downsides of this approach remains. One way of going around this problem is to train feature extractor in unsupervised manner and then tune the classification on a small labelled dataset. This approach is employed in [21] to solve the problem of anomaly detection in wireless communications.

Another approach for the labeling problem is employing transfer learning [15], [18]. In [18], object detection "You Only Look Once" (YOLO) model, pretrained on the ImageNet dataset, is tuned to detect and classify different types of transmissions using spectrograms. It is shown that the proposed model performs well in classifying interfering signals on simulated data with different signal-to-noise ratios and provides additional information about the position of the transmission events in the spectrum.

¹https://www.sigidwiki.com/wiki/Signal_Identification_Guide

²<https://log-a-tec.eu/datasets.html>

Table 1: Related works with main characteristics

| Publication | Problem type | Architecture | Data type | Dataset | Conti-nuous sensing (yes/no) | Labels (yes/no) | Approach | Band |
|-------------|---|----------------------|-------------------------|--------------------------------------|------------------------------|-----------------|--------------------------------|--------------------------------------|
| [5] | Modulation classification (<i>multiclass</i>) | LSTM | I/Q, PSD | RadioML, ELEC-trosense | Yes | Yes | Supervised | 174-230 MHz, 470-862MHz, 25-1300 MHz |
| [15] | Device fingerprinting (<i>multiclass</i>) | DCC | I/Q | DARPA, Synthetic | / | Yes | Supervised | 2.4GHz, 5GHz, 978MHz, 1090MHz |
| [16] | Device fingerprinting (<i>multiclass</i>) | CNN | I/Q | Test-bed | / | Yes | Supervised | 5GHz |
| [6] | Technology classification (<i>multiclass</i>) | DT, FNN, CNN | RSSI, I/Q, Spectrograms | Ghent, Dublin | Yes | Yes | Supervised | 5540MHz, 2412MHz, 806MHz |
| [17] | Modulation classification (<i>multiclass</i>) | CNN | I/Q | Test-bed, Synthetic | / | Yes | Supervised | 900MHz |
| [18] | Technology characterization trough object detection (<i>multiclass</i>) | YOLO CNN | Spectrograms | Test-bed, Ghent | Yes | Yes | Supervised | 5540MHz, 2412MHz, 806MHz |
| [19] | Device fingerprinting with clustering (<i>multiclass</i>) | CNN | I/Q | Test-bed | / | Yes | Semi-supervised | 0.25 - 1.25MHz, 1.67MHz, 2.5MHz |
| [20] | Device fingerprinting (<i>multiclass</i>) | DCC + CNN | I/Q | DARPA | / | Yes | Supervised, Unsupervised | 2.4GHz, 5GHz, 978MHz, 1090MHz |
| [7] | Anomaly detection (<i>binary</i>) | PredNet-autoencoder | Spectrograms | Synthetic | / | No | Unsupervised* | / |
| [21] | Anomaly detection (<i>binary</i>) | Supervised CNN-based | PSD | Synthetic, HackRF, SDR, Electrosense | Yes | Yes | Unsupervised | 10MHz-3GHz |
| [12] | Transmissions detection and classification (<i>binary</i>) | Image processing | Spectrograms | Log-A-Tec | Yes | Yes | Unsupervised | 868MHz |
| Ours | Transmissions clustering (<i>multiclass</i>) | Deep-clustering | Spectrograms | Log-A-Tec | Yes | No | Unsupervised (Self-supervised) | 868MHz |

Although the semi-supervised and transfer learning are proven to lower the amount of data that is required for the training, labeled data is still needed for the tuning. Spectrum data content is not as universal as the RGB images and it is much more dependent on the operating environment regarding the noise, signal strength, fading, multipath effects, etc., which makes it necessary to provide labels for each specific radio environment.

2.3. Unsupervised learning

Considering the availability of large amounts of unlabelled spectrum data [11], [10], another approach to the labeling problem with high potential, which we consider as under-explored in the spectrum data processing domain, is using unsupervised models. We believe that the development of unsupervised approaches could more effectively solve the labeling problems and provide highly automated architectures that can be adapted to different operating environments with minimum expert intervention.

There are existing efforts in this direction, but they only consider the marginal cases of event detection (binary classification). A pipeline for automatic detection of wireless transmissions using classic image processing techniques is proposed in [12]. Another such example is the work in [22] where auto-encoder is utilized as feature learner for anomaly detection and

shown to outperform the robust principal component analysis (PCA).

In our work, we align with the efforts of developing completely unsupervised models that would provide feature learning in an automated manner. We develop a self-supervised architecture that can provide the functionality of simple activity detection, but also enable fine grain classification of wireless transmissions of different technologies in wireless spectrum data.

3. Architectures of the SSL and baseline systems

In this paper we investigate the suitability of SSL models to automatically cluster wireless spectrum activities identified from spectrogram segments, i.e., transmission events of different shapes and intensity levels. The models are developed using two different SSL systems and a baseline system. They assume no prior knowledge about the types and number of different spectrum activities present in the dataset, and there is also no ground truth or labeling available for the dataset used.

3.1. SSL architectures

As a reference SSL system we adopted the existing self-supervised DeepCluster architecture proposed in [14] for RGB image feature learning based on a VGG-16 (Visual Geometry Group) standard deep Convolutional Neural Network (CNN)

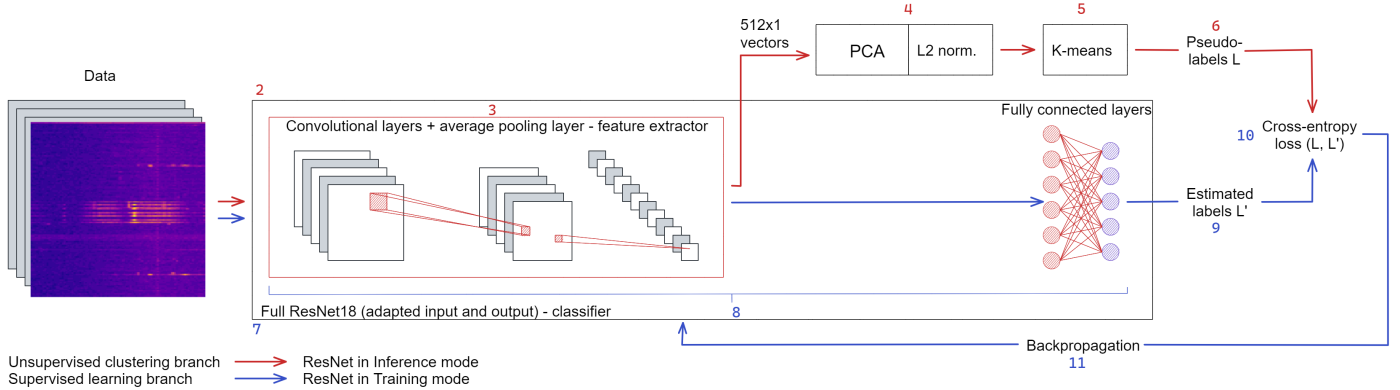


Figure 1: Architecture of the self-supervised CNN system.

architecture with batch normalization that is regularly used in computer vision applications. This system alternates between clustering the image features produced by CNN and updating its weights by predicting the cluster assignments.

Inspired by the approach of this reference system, we developed a SSL system depicted in Figure 1, which is actually an adaptation of DeepCluster for spectrum activity identification and clustering from spectrograms, characterized by much less content compared to RGB images, thus allowing for significant complexity reduction and performance optimization. As it can be seen from the figure, the system design contains two branches, (1) a so-called unsupervised branch depicted with red arrows and (2) a supervised branch depicted with blue arrows. Both branches contain a CNN-based feature extractor. In the unsupervised branch it is followed by a dimensionality reduction (PCA) and normalization (L2) preprocessing block and concluded with the K-means clustering block. In the supervised branch, the feature extractor is followed by fully connected layers as a classifier. Note that even if we refer to the second branch as supervised, it does not rely on actual labelled data. It relies on pseudo-labels that are repeatedly generated by K-means in unsupervised branch and refined through feedback, i.e. backpropagation. By working in tandem, the two branches realize self-supervision.

Compared to the original DeepCluster architecture, we propose the following adaptations:

- Motivated by the findings in [17], rather than using VGG as a CNN deep learning architecture, we select ResNet architecture as it was shown to perform better in a supervised task of modulation classification. As we show later, with ResNet we achieve very similar performance as with VGG at significant complexity reduction by roughly 12 times less trainable parameters.
- From the ResNet family we use ResNet18 (18 showing the number of convolution layers in CNN) in its original form, but with input and output layers customized according to the shape of the images and the number of classes, i.e., a single input channel in the case of spectrogram images compared to a 3-channel input required for RGB images that ResNet18 was originally designed for.

- We also added PCA feature space reduction before clustering to adapt to the significantly lower amount of content in spectrograms compared to RGB images.

Further in the paper, we refer to the VGG-based and ResNet-based self-supervised models as SSL-VGG-X and SSL-RN-X, respectively, with X representing the number of PCA components used for the model instance development.

The pseudo-code corresponding to the workflow of the proposed self-supervised system is given in Algorithm 1. For clarity and clear mapping, the blocks of the system in Figure 1 are marked with the corresponding line numbers from the pseudo-code in Algorithm 1.

3.1.1. Workflow of the unsupervised branch

In the initial phase, the CNN is initialized randomly and the input data, which consists of image-like spectrum segments, is unlabeled. The clustering algorithm (unsupervised branch, marked with red arrows in Figure 1) is used to cluster the features and provide pseudo-labels (denoted by L in the figure) at the beginning of each training epoch. Initialization of the cluster centers is random. The features are extracted using the convolutional layers of the ResNet and the average pooling layer, which has the size of 512×1 (lines 2-3 in Algorithm 1). Thus, a descriptor in the form of 512×1 vector is obtained for each spectrum segment image. These descriptors are then PCA-reduced, L2-normalized and finally clustered (lines 4-5 in Algorithm 1).

3.1.2. Working of the supervised branch

In this phase, ResNet based CNN is used in training mode, as a supervised classification model. The flow of this pipeline activity is indicated by the blue arrows in Figure 1. Using the provided cluster assignments from the previous step as pseudo-labels (L) for the input images, the ResNet architecture is trained for one epoch. This completes one iteration of the entire pipeline work cycle.

The procedure stops when the predefined number of iterations (training epochs) is reached. In our experiments, we used 200 training epochs. This number was determined empirically by observing the convergence of the loss function.

Algorithm 1 Workflow of the architecture

```
1: while Iteration < NumberOfEpochs do
  Unsupervised branch:
2: ResNet ← EvaluationMode
3: ExtractFeatures      ▶ ResNet convolutional layers
4: ProcessFeatures     ▶ PCA + L2 norm.
5: ClusterFeatures    ▶ K-Means
6: (L)Pseudo-labels ← ClusterAssignments
  Supervised branch:
7: ResNet ← TrainingMode
8: EstimateLabels      ▶ ResNet as classifier
9: L' ← EstimatedLabels
10: Cross-entropy(L, L')
11: Backpropagation   ▶ Update ResNet weights
12: end while
```

3.2. Baseline system

Considering that the most influential part of the architecture is the feature learning component, we take PCA-based representation learning as a baseline for comparison with the SSL models complemented by a K-means clustering algorithm, as depicted in Figure 2. The system consists of a flattening block, PCA-dimensionality reduction and L2 normalization for input data preprocessing, followed by the K-means clustering block.

The flattening reorders the elements of the input matrix into a single row for each data sample. On the vectors provided by the flattening, the same sequence of operations is applied, as for the vectors provided by the self-supervised system. PCA is applied on the flattened data and as a result of this operation, reduced feature vectors representing the input data are obtained. These vectors are then L2-normalized and finally used as an input to the K-means clustering algorithm.

In the rest of the paper we refer to baseline models as B-PCA.

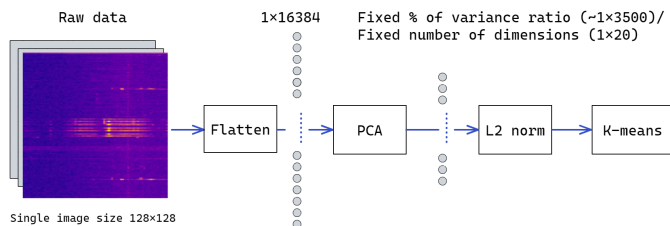


Figure 2: Architecture of the baseline system.

4. Methodology

In view of developing and benchmarking unsupervised spectrum activity exploration we define the methodological approach to prepare the raw data used to train the proposed self-supervised and baseline models, and to develop and evaluate high quality feature extraction, clustering and resulting models.

4.1. Raw training data preparation

The dataset used for the analysis consists of fifteen days of spectrum measurements acquired at a sampling rate of 5 power

spectrum density (PSD) measurements per second using 1024 FFT bins in the 868 MHz license-free (shared spectrum) SRD band with a 192 kHz bandwidth. The data is acquired in the LOG-a-TEC testbed. Details of the acquisition process and a subset of the data can be found in [11]. The acquired data has a matrix form of $1024 \times N$, where N is the number of measurements over time. By windowing the data with a window size W , the resulting raw images for training would have $1024 \times W$ dimension which can be computationally untractable for less capable computing platforms. Therefore, in addition to windowing in time, we are also windowing the dataset in frequency (i.e., FFT bins) direction.

The segmentation of the complete data-matrix into non-overlapping square images along time and frequency (FFT bins) is realized for a window size $W = 128$. An example of such segmentation containing 8 square images is shown in Figure 3, corresponding to image resolution of 25.6 seconds (128 measurements taken at 5 measurements per second) by 24 kHz. The window size is chosen to be large enough to contain any single type of activity and small enough to avoid having too many activities in a single image while also having in mind computational cost. Dividing the entire dataset of 15 days using $W = 128$ and zero overlapping, produces 423,904 images of 128×128 pixels, where the pixel values are scaled to the range between 0 and 1.

From previous work [12] we obtained labels of part of the transmissions in the employed dataset provided by experts. The labels are bounding boxes around transmissions in the same spectrogram data. We adapt these labels to our use case, considering the data is segmented in square-shaped regions. Each label as a rectangular region in the data matrix covers at least one square segment. All of the square segments that are overlapping with the labeled regions are marked as active, i.e., containing transmission(s). Thus we obtained labeled subset of square-shaped spectrograms that contain transmissions, as marked by experts, which have been used for the subsequent evaluation of the compared models.

The VGG-based model also requires adaptation on the dataset itself. In fact, using the described data segmentation in the SSL-VGG model, which was originally designed for input data size of 224×224 pixels, leads to converging the model to create only one cluster and zero valued feature vectors. To avoid this, we upscale the 128×128 spectrograms to the originally required input size for SSL-VGG. Another issue with SSL-VGG model is the number of training epochs. Running for too many (e.g., more than 40) epochs again leads to the behaviour explained above. The number of epochs that provides meaningful results with the SSL-VGG model was experimentally determined to be around 30, which is notably less than the number of epochs required for the SSL-RN model. We assume that the reason for such behaviour is the low amount of content in the spectrograms compared to the content-rich RGB images that the SSL-VGG architecture was originally designed for.

4.2. Feature development and evaluation methodology

As shown in Figure 1, the segmented and normalized raw data is passed through a feature extractor (ResNet18) and PCA/L2

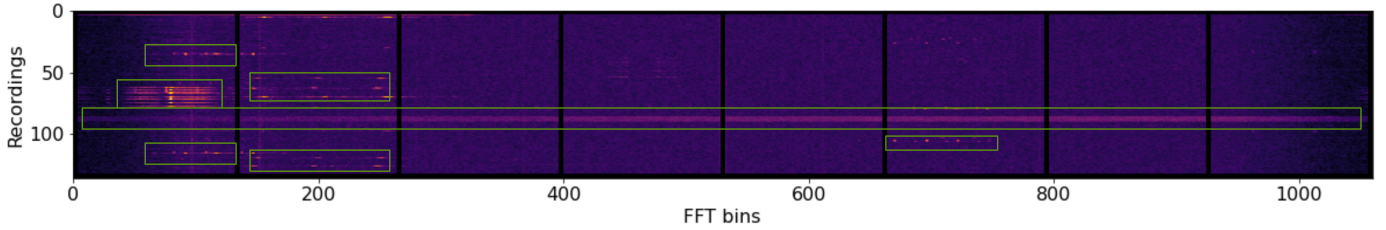


Figure 3: Sample of 8 spectrogram segments from the data.

preprocessing, before being actually clustered. These blocks, together, learn to engineer features. The better the quality of the engineered features that train the K-means clustering algorithm, the better the resulting clustering model. Therefore, in the process of developing the proposed self-supervised model, the feature development process needs to be tuned and evaluated.

While the feature extractor is automatically trained, the PCA performing dimensionality reduction for both the proposed self-supervised and the baseline system needs to be configured. We first analyze how many PCA components are needed to keep the most relevant information while discarding as much noise as possible. The number of dimensions D used in the PCA-reduced dimensionality representation is determined by setting a threshold on the amount of Explained Variance Ratio (EVR). We assume that the important information is encoded in much smaller number of dimensions (i.e., between 10 and 20 out of 512) because, contrary to the RGB images from the reference application of SSL model [14], the spectrograms contain much smaller amount of content. Visual analysis of the spectrograms shows that the transmission bursts surface is varying relative to the spectrogram size, but it is not bigger than around 10%, i.e., 1600 pixels of the spectrogram relative to its size of $128 \times 128 = 16384$ pixels. The EVR threshold is determined by exploring the plot of the cumulative sum of EVR of the PCA-transformed space dimensions.

Clusterability of developed features can be evaluated with different metrics such as the Hopkins score [23] and visual assessment of clustering tendency (VAT) [24]. The Hopkins score is a metric that shows the probability that randomly sampled subset of the data comes from a uniform distribution. Resulting values are between 0 and 1, with 0 meaning the data is not uniformly distributed. However, having nonuniform distribution does not guarantee existence of clusters in the data. One such case is if the data has normal distribution, which will show low Hopkins score but will not contain any meaningful clusters. To prevent possible false conclusions derived based on this metric alone, we also use the evaluation with the VAT algorithm, which produces matrix visualisation of the dissimilarity of samples based on their pairwise euclidean distances. The value of each element of the visualization matrix is proportional to the pairwise dissimilarity between each of the samples to all of the other samples. Thus, the left diagonal of the matrix is with zero values representing dissimilarity of each sample to itself. The samples are ordered in such a way that groups that are located close in the feature space, according to the distance metric, ap-

pear as dark squares along the diagonal of the matrix. Implementation wise, an improved version of the VAT (iVAT) is used, which provides better visualization than the standard one.

In the evaluation process, the Hopkins score and the VAT plots are complementary and will be considered both at once, since VAT does not provide quantification, while the Hopkins score alone only gives an information about the uniformity of data distribution and not on its clusterability.

4.3. Cluster development and evaluation methodology

To develop the cluster model that best finds similar transmissions, the compared architectures have to be trained several times for different values of k in K-means resulting in as many models. These models then need to be evaluated to see which one contains the cleanest clusters, i.e. provides clear data separation. As all the possible transmissions that may occur are not known in advance, we choose $k \in [2, 3, 4, \dots, 30]$.

The clustering is then evaluated with two standard metrics, the Silhouette score [25] and the Davies-Bouldin index [26], and also manually by cluster analysis and explanation.

The Silhouette score is a value that measures the quality of the clustering by evaluating how similar is each sample to its assigned cluster. The values it takes are in the range of $[-1, 1]$, where bigger values mean better clustering. Silhouette score of a cluster is the average of the scores of its elements, while Silhouette score of a clustering is the average of the scores of all of the clusters.

The Davies-Bouldin index is a clustering quality metric calculated as average of the similarity value of each cluster to its most similar (closest) cluster. The range of values that this metric takes has only lower bound 0 and smaller values mean better clustering.

As discussed in Section 3, the clustering algorithm is randomly initialized, so labels are not fixed to any specific type of content. Thus, besides the quantitative evaluation of the quality of the clustering results, manual evaluation is also performed in order to interpret the content that is specific for each cluster together with the frequency that is specific for the content. The motivation for the manual inspection is to verify that the clusters formed as output of the K-means are meaningful subsets of spectrograms containing highly correlated types of spectrum patterns (transmissions). Evaluation is made on plots of averaged spectrograms and histograms of frequency locations specific for the cluster's samples.

4.4. Evaluation with labeled data

After manual evaluation we can assign specific type of transmission to each of the formed clusters. Also, it is justified to expect that there will be clusters with empty/no transmission segments since the dataset is created by uninterrupted measurements from certain time period and it is hardly possible that each spectrogram will contain transmission. This is verified by visualization of sample data. Knowing this, we evaluate the models by utilizing the created labeled data, as explained in Section 4.1, and check how well the models are performing for the task of activity detection. The evaluation is made by running the labeled spectrograms containing transmission through the trained models and calculate the percentage of them that were correctly distributed across the clusters that contain transmissions, marked in the previous step of manual evaluation. Correct classifications would be labeled samples assigned to any of the transmissions-rich clusters and misclassifications would be labeled samples assigned to the empty/no activity clusters.

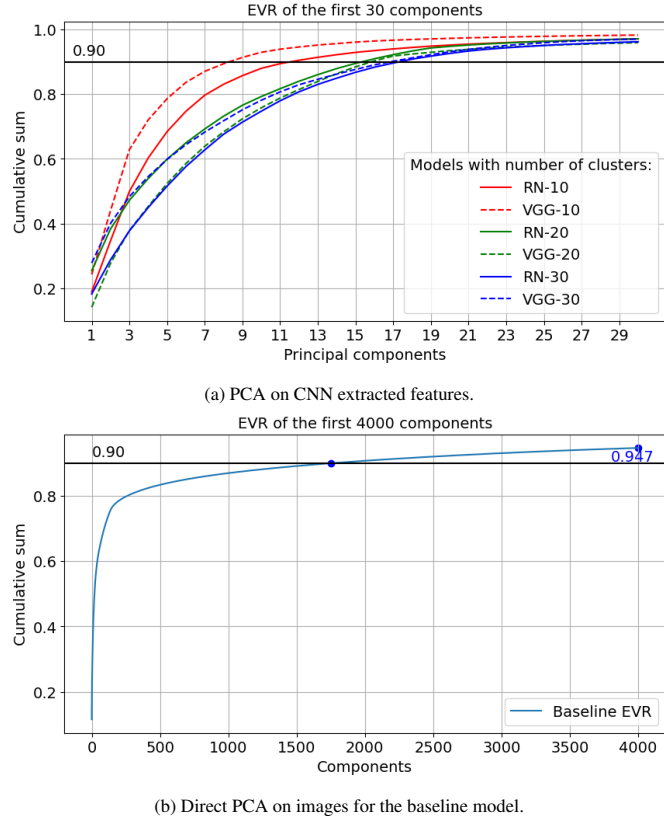


Figure 4: EVR of the features after the application of PCA.

5. Experimental results

We started the performance evaluation with the analysis of the feature space of a few experimentally trained models to provide an insight about the content dynamics of the specific range of PCA components before we continued with the investigation of the number of clusters in the dataset, and set the number of

PCA components to be used in clustering. Using the methodology proposed in previous section we carried out a number of experiments to compare the performance of SLL and baseline models, and eventually we showcased the suitability of SSL models for two representative use cases.

5.1. Effect of the dimensionality reduction

For configuring the PCA-based dimensionality reduction of the proposed self-supervised and baseline models, we first explored the cumulative sum of the EVR of the features, as shown in Figure 4, for the different models. Figure 4a plots EVR of three different models corresponding to 10, 20 and 30 clusters trained with SSL-VGG (dashed lines) and SSL-RN (solid lines) architectures, respectively. It can be seen that 90% of the EVR is contained in at least 17 components across the models and that there is no significant change in the EVR when considering more than 20 components. Therefore we selected the first 20 PCA components as the size of the vectors encoding the input images, which are also input for the K-means algorithm in the unsupervised branch in Figure 1.

The plot in Figure 4b represents the feature space for the baseline model. It can be seen that direct PCA on images requires 1752 components to keep 90% EVR independent of the final number of clusters. Taking this into consideration we used two baseline models, one with 1752 and one with 20 (i.e. the same as with SSL models) PCA components, and we refer to them in the following as B-PCA-2k and B-PCA-20, respectively.

Comparison of results in Figures 4a and 4b shows that SSL models are able to learn to encode the relevant information for cluster development in less than 1% of the PCA components required by the baseline model for the same 90% EVR. Thus, self-supervision provides significant simplification of further processing because of the dimensionality reduction, i.e. by two orders of magnitude.

5.2. Clustering tendency of the features

Using SSL-VGG-20, SSL-RN-20, B-PCA-2k and B-PCA-20 derived in the previous section as input features to the K-means clustering in both models, we perform quantitative evaluation of how suitable are the resulting features for clustering.

The Hopkins scores evaluating the quality of the features using the SSL versus the baseline models are presented in Figure 6. For the baseline models B-PCA-20 and B-PCA-2k, the clusterability is independent of the number of clusters so we expect to have constant values. The small variations of the yellow and green curve are due to random initialization of the Hopkins calculation procedure. This is not the case for the SSL models since the number of clusters is always the same as the number of classes of the CNN output, thus affecting the CNN architecture.

The SSL-VGG-20 (red line) has consistently the best performance across the different models. The scores of the proposed SSL-RN-20 (blue line) are close to the B-PCA-20 for models with up to 10 clusters, they improve for models with the number of clusters between 10 and 20, and are close to SSL-VGG-20 for models with 20 to 25 clusters.

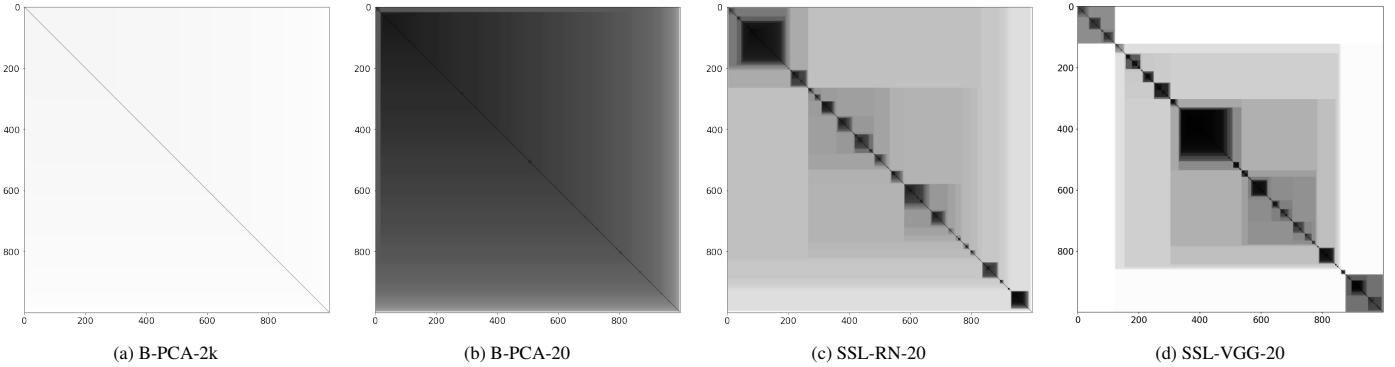


Figure 5: VAT plots of the different feature vectors.

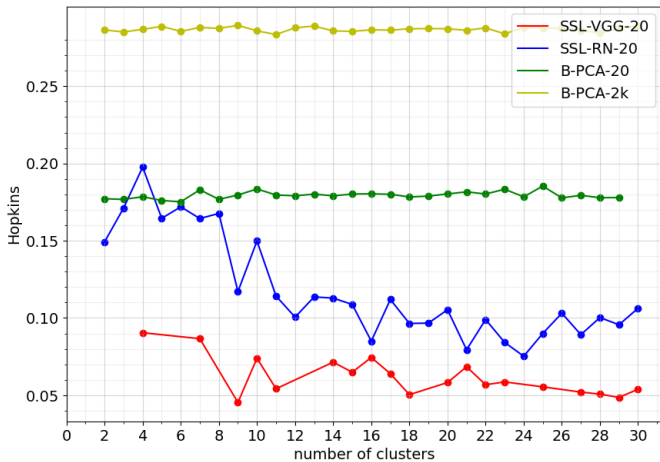


Figure 6: Hopkins scores of the extracted features.

For further evaluation, we selected the SSL models with 23 clusters since they are in the range of best models for both considered architectures. For models with 23 clusters we next considered the VAT plots of the selected SSL and baseline models given in Figure 5. Figure 5a corresponding to B-PCA-2k contains no grouping at all, meaning that the feature vectors provided by this model are randomly distributed in the feature space. Figure 5b corresponding to B-PCA-20 shows that there is only a small grouping in the left upper corner, which justifies the better performance compared to the B-PCA-2k on the Hopkins evaluation. Figure 5c shows the clustering tendency of the features obtained with SSL-RN-20. There are around 20 distinguishable squares corresponding to groups of highly correlated samples. This confirms good scores on the Hopkins evaluation achieved by SSL-RN-20 models with 20 to 25 clusters. For the SSL-VGG-20, the feature space contains three well separated, highly correlated groups of features and comparable size and number of darker squares as for the SSL-RN-20. The three well separated groups are the reason for the consistently better Hopkins scores of the SSL-VGG-20 compared to others, considering the Hopkins’s definition. However, the number and size of visually distinguishable dark squares of the SSL-VGG-20 is comparable with the SSL-RN-20, suggesting that similar number of clusters could be existing in both feature spaces.

From this section we can conclude that the PCA-only baseline models are not capable of encoding significant number of groups of correlated features from the input spectrograms. Following this conclusion, we only used the B-PCA-20 for further comparisons, since the B-PCA-2k feature vectors showed no clustering tendency at all, making their further evaluation irrelevant.

5.3. Evaluation of clusters quality

Evaluating the clustering quality is performed according to the methodology described in Section 4.3. For the Davies-Bouldin scores plotted in Figure 7a, it can be seen that the SSL models, SSL-RN-20 and SSL-VGG-20 have consistently better scores compared to the baseline model B-PCA-20 for any model trained with 6 or more clusters. Considering the SSL models only, the proposed SSL-RN-20 shows comparable or better performance than SSL-VGG-20.

The Silhouette score evaluation indicates the same pattern as the Davies-Bouldin score. The proposed SSL-RN-20 shows comparable or only slightly worse performance than SSL-VGG-20 and significantly better than B-PCA-20. This observation supports our conclusion from the previous section, which evaluated the clustering tendency of the features, that both SSL models have comparable groupings in the feature space and are significantly better than the PCA-only models.

5.4. Analysis of clusters

According to Sections 5.2 and 5.3, models with 20 to 25 clusters are providing the best results on the used dataset. Considering this advantage of using the SSL architectures over the baseline clustering approach, we present two use cases where the learning capabilities of such model are being exploited.

1. Transmission detection, where we group the activity-rich clusters containing transmissions as single class, and the clusters with spectrograms that do not contain transmissions as a second class.
2. High granularity clustering, considering all of the existing shapes appearing in the formed clusters.

Statistics of the three compared models are summarized in Table 2. Complementary to the table, Figure 8 provides the average spectrograms and histograms of frequency sub-bands

Table 2: Statistics of the clusters. Legend: yellow-Stripes, red-Dotted, blue-Edges, gray-Idle, green-High intensity, white-Undefined

| B-PCA-20 | | | | SSL-VGG-20 | | | | SSL-RN-20 | | | |
|--------------|----------------|---------------------|----------------|------------|----------------|---------------------|---------------|------------|----------------|---------------------|---------------|
| Cluster ID | Cluster size % | Mean IC image dist. | Mean IC dist. | Cluster ID | Cluster size % | Mean IC image dist. | Mean IC dist. | Cluster ID | Cluster size % | Mean IC image dist. | Mean IC dist. |
| 1 | 30.32 | 0.00395 | 0.02745 | 4 | 14.0 | 0.00007 | 0.13943 | 9 | 6.28 | 0.00032 | 0.33915 |
| 7 | 10.2 | 0.00267 | 0.03576 | 5 | 7.23 | 0.00016 | 0.35096 | 10 | 6.19 | 0.00034 | 0.35764 |
| 18 | 8.97 | 0.00420 | 0.02172 | 17 | 5.66 | 0.00017 | 0.37488 | 17 | 6.1 | 0.00006 | 0.27932 |
| 9 | 3.75 | 0.00426 | 0.04554 | 3 | 5.34 | 0.00016 | 0.32649 | 8 | 5.77 | 0.00033 | 0.50665 |
| 6 | 3.66 | 0.00435 | 0.03903 | 6 | 5.34 | 0.00015 | 0.27536 | 1 | 5.75 | 0.00033 | 0.38822 |
| 22 | 3.49 | 0.00447 | 0.04674 | 15 | 5.12 | 0.00016 | 0.29993 | 5 | 5.61 | 0.00036 | 0.35694 |
| 10 | 3.4 | 0.00432 | 0.04636 | 12 | 5.08 | 0.00016 | 0.27939 | 13 | 5.48 | 0.00033 | 0.31041 |
| 16 | 3.19 | 0.00441 | 0.04210 | 18 | 4.67 | 0.00035 | 0.54160 | 4 | 5.48 | 0.00010 | 0.23226 |
| 12 | 3.16 | 0.00452 | 0.04384 | 1 | 4.57 | 0.00036 | 0.47015 | 2 | 5.12 | 0.00043 | 0.40095 |
| 8 | 3.14 | 0.00433 | 0.04234 | 13 | 4.52 | 0.00055 | 0.53001 | 6 | 5.1 | 0.00040 | 0.38268 |
| 13 | 2.88 | 0.00429 | 0.03622 | 8 | 4.44 | 0.00018 | 0.49788 | 14 | 4.76 | 0.00037 | 0.36960 |
| 14 | 2.84 | 0.00451 | 0.04625 | 9 | 4.38 | 0.00042 | 0.42296 | 21 | 4.73 | 0.00047 | 0.55252 |
| 19 | 2.76 | 0.00441 | 0.04409 | 0 | 4.09 | 0.00008 | 0.18563 | 15 | 4.57 | 0.00029 | 0.40767 |
| 17 | 2.7 | 0.00414 | 0.03665 | 14 | 3.82 | 0.00017 | 0.38345 | 19 | 4.5 | 0.00057 | 0.40138 |
| 21 | 2.68 | 0.00463 | 0.05222 | 19 | 3.75 | 0.00017 | 0.35269 | 16 | 3.94 | 0.00010 | 0.48463 |
| 20 | 2.28 | 0.00461 | 0.04978 | 10 | 3.3 | 0.00040 | 0.33257 | 3 | 3.7 | 0.00015 | 0.46470 |
| 11 | 2.04 | 0.00461 | 0.04799 | 16 | 3.29 | 0.00035 | 0.44356 | 20 | 3.26 | 0.00036 | 0.54420 |
| 15 | 2.04 | 0.00463 | 0.05114 | 2 | 3.22 | 0.00039 | 0.48657 | 22 | 3.11 | 0.00045 | 0.36406 |
| 5 | 1.98 | 0.00448 | 0.04710 | 11 | 3.02 | 0.00108 | 0.55814 | 11 | 2.34 | 0.00036 | 0.50662 |
| 4 | 1.87 | 0.00465 | 0.04884 | 22 | 2.24 | 0.00318 | 0.55121 | 12 | 2.31 | 0.00041 | 0.38436 |
| 0 | 1.64 | 0.00428 | 0.04072 | 20 | 1.28 | 0.00309 | 0.32611 | 18 | 2.11 | 0.00330 | 0.47227 |
| 3 | 0.84 | 0.00472 | 0.04858 | 21 | 0.88 | 0.00041 | 0.59800 | 0 | 2.07 | 0.00030 | 0.58840 |
| 2 | 0.18 | 0.00281 | 0.04853 | 7 | 0.76 | 0.00045 | 0.34755 | 7 | 1.7 | 0.00006 | 0.41976 |
| Overall mean | | 0.00427 | 0.04300 | | | 0.00055 | 0.39454 | | | 0.00044 | 0.41367 |
| Overall std | | 0.00051 | 0.00733 | | | 0.00083 | 0.11895 | | | 0.00062 | 0.08748 |

for the samples of each cluster. Cluster statistics in Table 2 contains the cluster sizes in percentages of the entire dataset (*Cluster size %*), euclidean distances of the assigned samples to the corresponding cluster centers in the feature space using the 1×20 vectors (*Mean IC image dist.*) and image mean-squared-error similarities between each cluster’s average spectrogram and the spectrograms of its assigned samples (*Mean IC dist.*).

Interestingly, the B-PCA-20 has the lowest *overall mean of inter-cluster (IC) distances*, one order of magnitude lower than the SSL models. But, this is a result of having small variance ratio contained in the 20 dimensions of the PCA transformed space of the raw images (baseline PCA approach), and to note again, using bigger amount of components resulted to even worse results in Section 5.2. On the other hand, the IC image distances are one order of magnitude worse compared to the SSL models, which confirms the performance seen in Section 5.3. SSL-VGG-20 has slightly better *overall mean IC distance* than SSL-RN-20, which corresponds to better distinguishing of the features according to Figure 6. However, for the *overall mean IC image distances*, SSL-RN-20 shows better performance with 0.00044 versus 0.00055 of SSL-VGG-20. This means that although the encoded features are better grouped by the SSL-VGG-20, the differences between the clustered spectrograms are actually bigger than the ones from the SSL-RN-20, thus showing that the later has slight advantage in groping wireless transmissions with similar shapes.

5.5. Manual evaluation

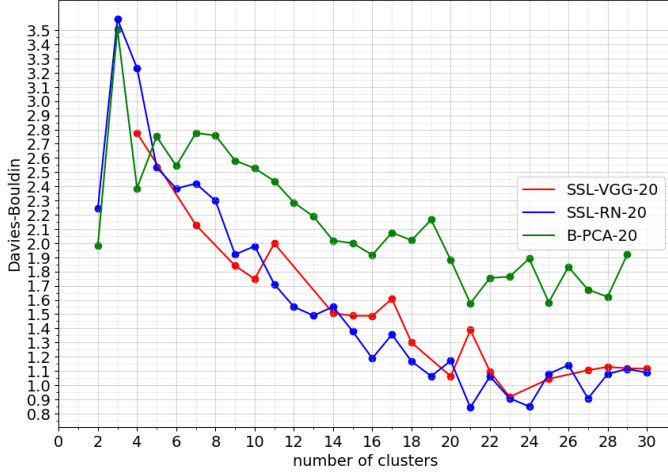
Manual evaluation for the selected models with 23 clusters relies on the distribution of samples per cluster with the relevant cluster statistics in Table 2 and the average spectrogram corresponding to each cluster in Figure 8. Averaging of spec-

trogram samples leads to highlighting the position of the most common types of activities that appear in each of the clusters. This visualization reveals which type of spectrum activity (i.e. transmissions of existing wireless technologies) corresponds to each of the clusters. So, instead of labeling large amounts of data, we only need to analyse the content of the formed clusters. Since the B-PCA-20 model has shown weak clustering performance according to all previous metrics, manual evaluation was performed only on the clusters obtained with the SSL models.

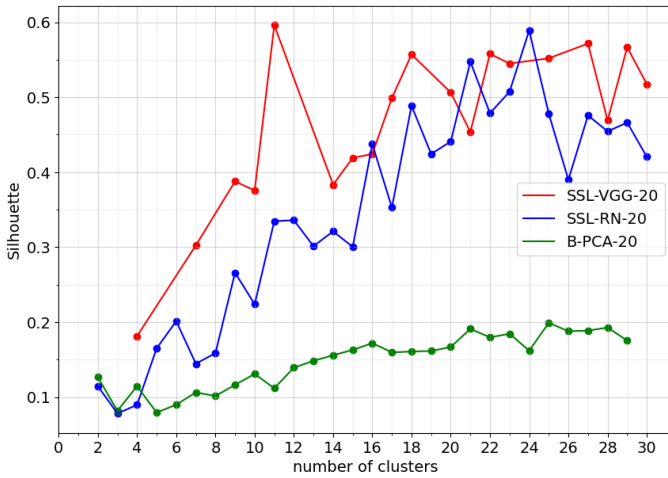
Based on the activity shapes and frequency histograms, clusters from both models can be separated in six major groups: Weak/no activity clusters, Left edge clusters, Right edge clusters, Strong activity, Dotted activity, and Horizontal stripes activity.

Weak activity is represented by cluster 4 for SSL-VGG-20 and clusters 7, 16 and 17 for the SSL-RN-20, containing 14% and 11.74% of the data, respectively. This means that there is a slight difference in the number of samples assigned to no activity clusters between the models.

The Left edge and Right edge clusters are mainly formed by samples from the edges (left-most and right-most) of the observed bandwidth (also shown on the histograms under each averaged spectrograms). The varying sensitivity of the sensor towards the edges of the bandwidth appears as highly influential information for both SSL models. The SSL-VGG-20 has clusters 9, 10 and 13 from the Left edge of the bandwidth, totaling 12.2% of the whole data which matches nearly perfect with $1/8=12.5$ of the data falling in the left-most sub-band (the entire bandwidth being separated in 8 sub-bands). The Right edge cluster formed by clusters 0, 11 and 17, totaling 12.77% of the data, follows the same pattern. Although it is evident that these



(a) Davies-Bouldin scores



(b) Silhouette scores

Figure 7: Evaluation curves of metrics for quality of clustering.

clusters also contain additional content (e.g. clusters 9, 10, 13), it is clear that the most prominent shape is the varying intensity background noise. This means that for these bandwidth regions, SSL-VGG-20 is focused more on the background noise than the transmission activity. For the SSL-RN-20, the Left edge and Right edge spectrum samples are contained in only two clusters, labeled 2 and 4, with roughly equal size of 5.12% and 5.61% of the total data, respectively. This means that the varying noise is also important for the SSL-RN-20, but more weight is given to the wireless transmission activities.

Considering the Strong activity samples, for SSL-VGG-20 they are distributed in clusters 20 and 22 (totaling 3.52%) while for SSL-RN-20 they are only in cluster 18 (2.11%). For this activity SSL-VGG-20 achieves better clustering. Based on the histogram of cluster 19 which has higher number of samples in the 7th sub-band, exactly where these activities appear according to the histogram of cluster 18, SSL-RN-20 is confusing the high intensity activity with the horizontal stripe activity in cluster 19.

Looking at the Dotted activity samples, contained in clusters

1, 2, 7, 16 and 18 for SSL-VGG-20 and in cluster 8 for SSL-RN-20, we observe that SSL-VGG-20 focuses much more on these patterns, ignoring the coexistence of other types of activities in the spectrograms. The histograms show that samples from these clusters contain all of the samples of the second sub-band, including those belonging to the Horizontal stripes activity which should obviously appear across the entire bandwidth as indicated in Figure 3. This is also confirmed by the histograms of the Horizontal stripes activity which are expected to be distributed along the entire bandwidth, but they are only in the sub-bands 3-7, confirming misclassification of the Dotted activity samples. On the other hand, SSL-RN-20 focuses much more on the Horizontal stripes activity samples, forming many clusters based only on the vertical location of the activity and having well distributed histograms across all sub-bands, as one would expect. Most of the samples that contain the Horizontal stripe and the Dotted activity samples are thus classified in the clusters with the Horizontal stripes (e.g. clusters 0, 11, 12 and 20).

We again confirm that both architectures show comparable performance, both having similar pros and cons, the difference is that they focus on different shapes of activities, so samples containing multiple transmissions are distributed across different clusters, predominantly the Dotted activity for SSL-VGG-20 and the Horizontal stripes activity for SSL-RN-20.

5.5.1. Use case 1 - Transmissions detection

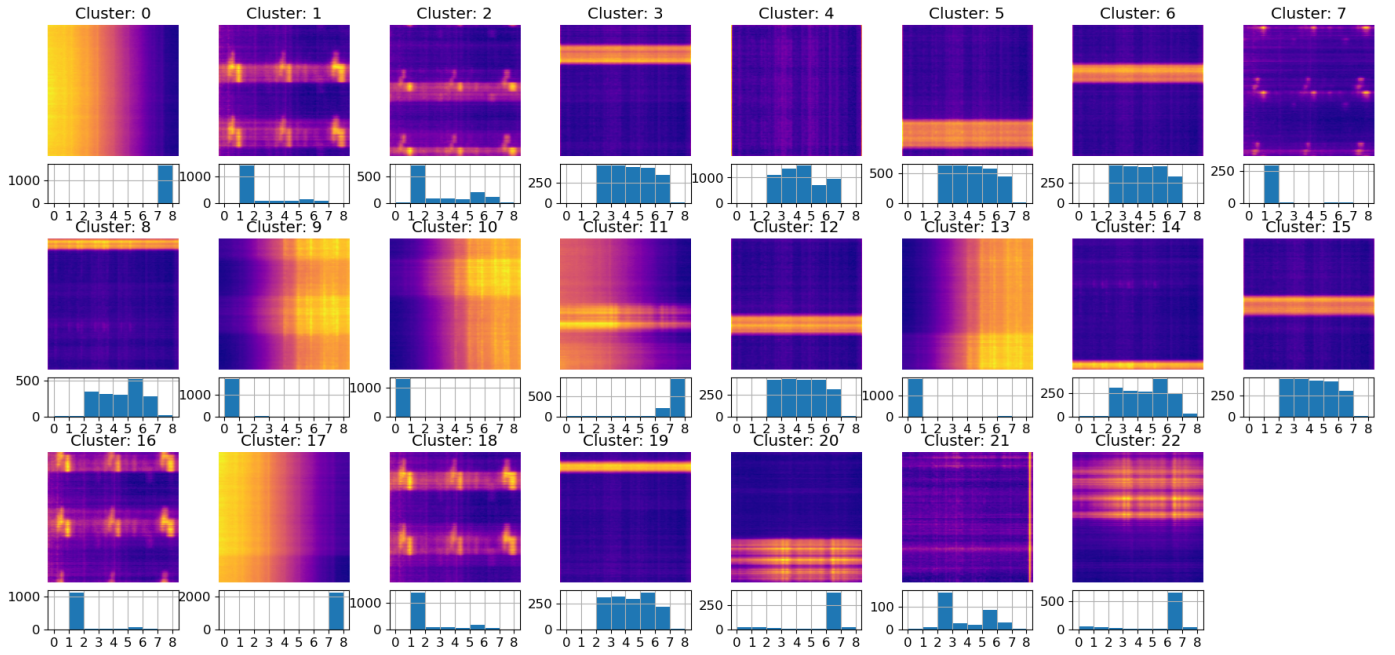
This use case is equivalent to binary classification of the labeled (positive) samples between the two groups of clusters which represent the Idle state and the Occupied state.

Idle state - No/weak spectrum activity. According to Figure 8, clusters with labels 7, 16, 17 for SSL-RN-20 and 4 for SSL-VGG-20, contain no or very low activity (*idle*). These clusters represent the parts of spectrum where no transmissions are recorded, or the sources of the signals are very distant so the signal intensity is very low. In the context of spectrum availability, they could be considered very similar since in both cases there are no existing patterns of transmissions with significant intensity.

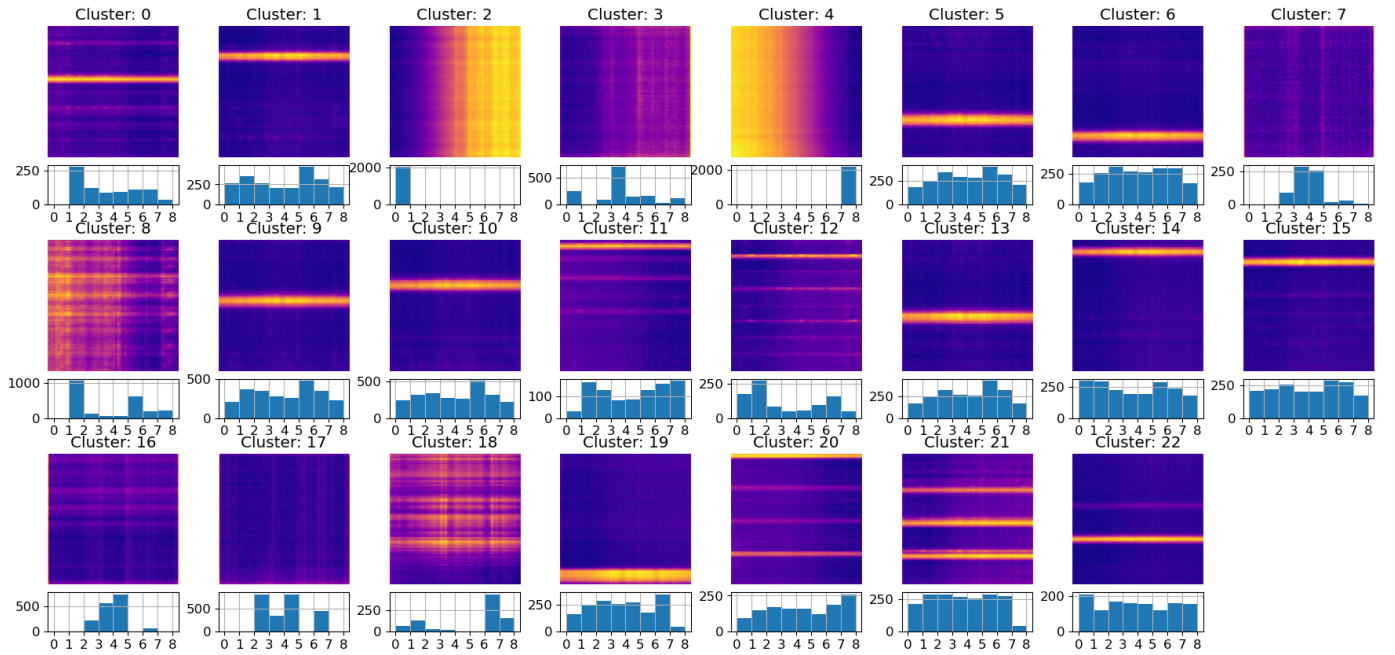
Occupied - presence of transmissions. All other clusters, 20 for the SSL-RN-20 and 22 for the SSL-VGG-20, contain some type of activity, so in the sense of spectrum availability they represent occupied spectrum segments. By considering the counts in Table 2, it can be seen that these amount to 88% (SSL-RN-20) and 86% (SSL-VGG-20) of spectrograms that contain at least one transmission. This represents valuable information about the spectrum occupancy that was extracted in automatic way and all the manual work is reduced to inspection of the averaged clusters' spectrograms.

5.5.2. Use case 2 - Distinguishing types of activities

The cluster contents and the cluster size allow for better understanding of types of activities and frequency of their appearance across the monitored radio spectrum. Considering only the



(a) SSL-VGG-20



(b) SSL-RN-20

Figure 8: Average spectrograms and frequency histograms of appearance for each cluster.

low-activity clusters, we acknowledge the percentage of available slots for transmission during time. Analog to this, there are also percentages for other types of activities. This means that information is provided about what portion of the spectrum is occupied with certain types of activity or combination of overlapping activities. This is useful when more granular separation of the spectrograms is required. The mentioned manual evaluation of the averaged spectrograms has a crucial role in such case. For this use case we only exemplify the SSL-RN-20 model with 23 clusters.

The clusters containing different types of combined activities can be considered as separate classes. In this way, besides the information for the spectrum occupancy, additional information can be derived for the frequency of occurrence and types of overlapping transmissions. In summary, based on manual evaluation of the clusters in Section 5.5, the number of activity types can be reduced to 6, including the *Idle* type of clusters containing 11.74% of the total data.

Occupied - Horizontal stripes. According to the average spectrograms visualization in Figure 8b, there are several clusters with mostly horizontal stripes (clusters 1, 5, 6, 9, 10, 13, 14, 15, 19 and 22), which account for 51.35% of the dataset. These samples represent the same type of activity, namely IEEE 802.15.4 transmissions, that occupy the entire bandwidth covered with a single segment, and they last for short time with regards to the time duration of a single sample. The location of the stripe is varying in vertical direction because the segmentation of the data in non-overlapping windows is fixed, as explained previously in Section 4.1, without correlation to the appearance times of any of the activities.

Occupied state - Horizontal stripes + other types of activity. Second type of activities is observed when the same horizontal stripes appear combined with other activities (clusters 0, 11, 12, 20, and 21), representing 14.71% of the samples. Together they represent separate cluster of segments where multiple activities are occurring in the same spectrogram segment. Some of the activities we distinguish correspond to concurrent IEEE 802.15.4, proprietary and LoRA transmissions.

Occupied state - High intensity activity. Cluster 18 (2.11% of the data) contains strong activity spread along the time axis (vertical) direction. These activities correspond to LoRA transmissions. Many of this transmissions are also coexisting with the IEEE 802.15.4 transmissions, as discussed in Section 5.5.

Occupied state - Dotted activity. Cluster 8 (5.77% of the data) contains shapes of dotted activity that are apparent at various locations along the time (vertical) axis. Such activities correspond to LoRa and proprietary transmissions.

Edge sub-bands. It is important to notice that varying background noise is also influential in the clustering. Samples in clusters 2 and 4 contain significant amount of background noise, having weaker values on one side of the spectrogram and gradually increasing in horizontal direction (frequency axis). As a consequence of this, such spectrograms are clustered separately making up 10.6% of the data, which cannot be specified if it is occupied or not.

Table 3: Transmission detection performance and complexity comparison.

| Algorithm | SSL-RN-20 | SSL-VGG-20 | Dilate/erode [12] | TX grouping [12] |
|--------------------|-------------|-------------|-------------------|------------------|
| Precision % | 76.0 | 76.6 | 77.7 | 68.2 |
| Recall % | 93.6 | 94.1 | 86.3 | 94.7 |
| F1 % | 83.9 | 84.5 | 81.8 | 79.3 |
| Num. of parameters | 11 M | 133 M | / | / |

5.6. Evaluation with labeled data

We evaluate the performance of the two models for transmissions detection according to Section 4.4, feeding labeled samples of transmissions to the models and determining how

many of these samples were correctly distributed to clusters with present transmissions and clusters with no transmissions. Table 3 summarizes the evaluation. We also compare the proposed solution with existing transmission detection algorithms evaluated on the same dataset in [12]. Surprisingly, the *Dilate/Erode* achieves the highest precision score with 1.1pp margin and the lowest recall score with 6-7pp margin, while the *TX grouping* achieves the highest recall score with 0.6pp margin and the lowest precision with almost 8pp margin. This means that, although the *Dilate/Erode* has the highest ratio of real transmissions in the detected transmissions, it fails to detect significant amount (roughly 14%) of the total number of transmissions. On the opposite, the *TX grouping* detects the highest percentage of the total number of transmissions, but in the same time also classifying many of the *Idle* samples as samples with transmissions, causing poor precision.

Contrary to the *Dilate/Erode* and *TX grouping*, the SSL-based models show more balanced performance, considering the difference between the precision and recall, thus achieving higher F1 scores by margin of 2.1pp and 2.7pp for the SSL-RN-20 and SSL-VGG-20, accordingly. In general, the SSL-based models outperform the referenced ones on the task of transmission detection in continuously sensed spectrum data.

Comparing the SSL-based models, both of them show comparable performance, with slight advantage of the (original) SSL-VGG-20 (up to 0.6pp) across the metrics. Anyway, the proposed SSL-RN-20 achieves such performance by utilizing roughly 12 times less trainable parameters compared to the SSL-VGG-20, which could be a beneficial trade-of regarding the computing requirements for potential applications.

6. Conclusions

In the work presented in this paper, we investigated the suitability of SSL for automatic feature learning and clustering of real-world radio spectrum events making use of two SSL architectures, a state-of-the-art architecture SSL-VGG-20 originally developed for RGB image feature learning and its adaptation to the specifics of wireless spectrograms, a SSL-RN-20 architecture. We employed these architectures to develop SSL models with no labels and no prior knowledge, and compared their performance against the baseline model with PCA dimensionality reduction and K-means clustering. The comparison was first made for the evaluation of the clustering tendency of the input data with appropriately proposed metrics for the different models and the quality of the clustering results. The self-supervised models (SSL-RN-20, SSL-VGG-20) enable compact feature extraction, encoded in significantly lower number of dimensions (reduction is of two orders of magnitude) while preserving the same amount of EVR of the input features. They also outperform the baseline model in the clustering quality by 0.3 according to Silhouette scores, and by 0.6 according to Davies-Bouldin score. The study was supported also by manual evaluation based on visual inspection and evaluation by labeled data. Results show that SSL-based models outperform the existing transmission detection algorithms on continuously

sensed data by more than 2pp according to F1 scores. Additionally, our modification of the SSL-based architecture, utilizing ResNet type of CNN achieves comparable performance to the original implementation with VGG type of CNN while reducing the number of trainable parameters by 12 times.

Acknowledgments

This work was funded in part by the Slovenian Research Agency under the grant P2-0016. This work was funded in part by the Slovenian Research Agency under the grant P2-0016. This project has received funding from the European Union's Horizon Europe Framework Programme under grant agreement No 101096456 (NANCY). The project is supported by the Smart Networks and Services Joint Undertaking and its members.

References

- [1] Q. Zhao, B. M. Sadler, A survey of dynamic spectrum access, *IEEE signal processing magazine* 24 (3) (2007) 79–89.
- [2] V. Frascolla, A. J. Morgado, A. Gomes, M. M. Butt, N. Marchetti, K. Voulgaris, C. B. Papadias, Dynamic licensed shared access—a new architecture and spectrum allocation techniques, in: 2016 IEEE 84th Vehicular Technology Conference (VTC-Fall), IEEE, 2016, pp. 1–5.
- [3] X. Chen, J. Huang, Database-assisted distributed spectrum sharing, *IEEE Journal on Selected Areas in Communications* 31 (11) (2013) 2349–2361.
- [4] D. F. Külzer, S. Stańczak, M. Botsov, Cdi maps: Dynamic estimation of the radio environment for predictive resource allocation, in: 2021 IEEE 32nd Annual International Symposium on Personal, Indoor and Mobile Radio Communications (PIMRC), IEEE, 2021, pp. 892–898.
- [5] S. Rajendran, W. Meert, D. Giustiniano, V. Lenders, S. Pollin, Deep learning models for wireless signal classification with distributed low-cost spectrum sensors, *IEEE Transactions on Cognitive Communications and Networking* 4 (3) (2018) 433–445.
- [6] J. Fontaine, E. Fonseca, A. Shahid, M. Kist, L. A. DaSilva, I. Moerman, E. De Poorter, Towards low-complexity wireless technology classification across multiple environments, *Ad Hoc Networks* 91 (2019) 101881.
- [7] N. Tandiyaa, A. Jauhar, V. Marojevic, J. H. Reed, Deep predictive coding neural network for rf anomaly detection in wireless networks, in: 2018 IEEE International Conference on Communications Workshops (ICC Workshops), IEEE, 2018, pp. 1–6.
- [8] C. Zhang, P. Patras, H. Haddadi, Deep learning in mobile and wireless networking: A survey, *IEEE Communications surveys & tutorials* 21 (3) (2019) 2224–2287.
- [9] L. J. Wong, W. H. Clark IV, B. Flowers, R. M. Buehrer, A. J. Michaels, W. C. Headley, The rfml ecosystem: A look at the unique challenges of applying deep learning to radio frequency applications, *arXiv preprint arXiv:2010.00432* (2020).
- [10] S. Rajendran, R. Calvo-Palomino, M. Fuchs, B. Van den Bergh, H. Corcobés, D. Giustiniano, S. Pollin, V. Lenders, Electrosense: Open and big spectrum data, *IEEE Communications Magazine* 56 (1) (2017) 210–217.
- [11] T. Šolc, C. Fortuna, M. Mohorčič, Low-cost testbed development and its applications in cognitive radio prototyping, in: *Cognitive radio and networking for heterogeneous wireless networks*, Springer, 2015, pp. 361–405.
- [12] T. Gale, T. Šolc, R.-A. Moşoi, M. Mohorčič, C. Fortuna, Automatic detection of wireless transmissions, *IEEE Access* 8 (2020) 24370–24384.
- [13] L. Jing, Y. Tian, Self-supervised visual feature learning with deep neural networks: A survey, *IEEE transactions on pattern analysis and machine intelligence* 43 (11) (2020) 4037–4058.
- [14] M. Caron, P. Bojanowski, A. Joulin, M. Douze, Deep clustering for unsupervised learning of visual features, in: *Proceedings of the European Conference on Computer Vision (ECCV)*, 2018, pp. 132–149.
- [15] S. Kuzdeba, J. Robinson, J. Carmack, Transfer learning with radio frequency signals, in: 2021 IEEE 18th Annual Consumer Communications & Networking Conference (CCNC), IEEE, 2021, pp. 1–9.
- [16] S. Riyaz, K. Sankhe, S. Ioannidis, K. Chowdhury, Deep learning convolutional neural networks for radio identification, *IEEE Communications Magazine* 56 (9) (2018) 146–152.
- [17] T. J. O’Shea, T. Roy, T. C. Clancy, Over-the-air deep learning based radio signal classification, *IEEE Journal of Selected Topics in Signal Processing* 12 (1) (2018) 168–179.
- [18] E. Fonseca, J. F. Santos, F. Paisana, L. A. DaSilva, Radio access technology characterisation through object detection, *Computer Communications* 168 (2021) 12–19.
- [19] L. J. Wong, W. C. Headley, S. Andrews, R. M. Gerdes, A. J. Michaels, Clustering learned cnn features from raw i/q data for emitter identification, in: *MILCOM 2018-2018 IEEE Military Communications Conference (MILCOM)*, IEEE, 2018, pp. 26–33.
- [20] J. Robinson, S. Kuzdeba, J. Stankowicz, J. M. Carmack, Dilated causal convolutional model for rf fingerprinting, in: 2020 10th Annual Computing and Communication Workshop and Conference (CCWC), IEEE, 2020, pp. 0157–0162.
- [21] S. Rajendran, W. Meert, V. Lenders, S. Pollin, Saife: Unsupervised wireless spectrum anomaly detection with interpretable features, in: 2018 IEEE International Symposium on Dynamic Spectrum Access Networks (DySPAN), IEEE, 2018, pp. 1–9.
- [22] Q. Feng, Y. Zhang, C. Li, Z. Dou, J. Wang, Anomaly detection of spectrum in wireless communication via deep auto-encoders, *The Journal of Supercomputing* 73 (7) (2017) 3161–3178.
- [23] B. Hopkins, J. G. Skellam, A new method for determining the type of distribution of plant individuals, *Annals of Botany* 18 (2) (1954) 213–227.
- [24] J. C. Bezdek, R. J. Hathaway, Vat: A tool for visual assessment of (cluster) tendency, in: *Proceedings of the 2002 International Joint Conference on Neural Networks. IJCNN’02 (Cat. No. 02CH37290)*, Vol. 3, IEEE, 2002, pp. 2225–2230.
- [25] P. J. Rousseeuw, Silhouettes: a graphical aid to the interpretation and validation of cluster analysis, *Journal of computational and applied mathematics* 20 (1987) 53–65.
- [26] D. L. Davies, D. W. Bouldin, A cluster separation measure, *IEEE transactions on pattern analysis and machine intelligence* (2) (1979) 224–227.